Anisotropic moment tensor inversion and visualization applied to a dual well monitoring survey

Scott Leaney, Xin Yu, Chris Chapman, Les Bennett, Shawn Maxwell, Jim Rutledge, Schlumberger Microseismic Services; John Duhault, Lightstream Resources

Summary

In this paper we review the workflow used for anisotropic moment tensor inversion and visualization applied to a dual well monitoring survey from the West Pembina field in Alberta. The workflow makes use of an exact, dynamic layered VTI ray-tracer that allows for constant dip. Included are a description of VTI model calibration, moment tensor inversion, moment tensor decomposition and visualization. Interpretation of the results is ongoing.

Introduction

The source mechanism of induced microearthquakes is of interest to the oil and gas industry because of what it may reveal about the hydraulic fracturing process. The process of recovering the source mechanism of earthquakes is known generally as "moment tensor inversion", and techniques have been published applied to microseismic events (Urbancic *et al.*, 1996, Trifu *et al.*, 2000, Nolen-Hoeksema and Ruff, 2001, Eisner *et al.*, 2010). These techniques have made use of a time domain isotropic ray theory Green function. Full waveform approaches for the moment tensor inversion problem have also been studied, using finite-difference Green function computations in isotropic media (e.g. Kim, 2011). Due to the computational burden, compressive sensing techniques have been investigated for waveform inversion (Vera Rodriguez *et al.*, 2012). Rössler *et al.* (2007) described a time-domain inversion for earthquake sources in anisotropic media using ray theory Green functions, but the mechanism considered was limited to a displacement discontinuity source, which is an incomplete moment tensor. Recently a frequency domain inversion for the complete moment tensor was described (Leaney *et al.*, 2011; Leaney and Chapman, 2013) that makes use of anisotropic Green functions computed with a VTI ray tracer. In that work anisotropy was found to have a significant distorting effect on the inverted source mechanism. In this paper we describe a time-domain moment tensor inversion that makes use of the same VTI ray tracer for the Green function. We review the workflow on a real dual well monitoring job from the West Pembina field in Alberta. Included are a description of VTI model calibration, moment tensor inversion, moment tensor decomposition and visualization. Interpretation of the results is ongoing.

Forward problem

Consider far-field vector recordings of particle displacements at receiver location x_j, $u(t, x_j)$, for a source at location x_S. In the geometrical ray approximation (Chapman, 2004):

$$u(t, x_j) \cong \left[\sum_k^{rays} s(t) * \hat{g}_{kj} G_k(t, x_j) E_k \right] : M \qquad (1)$$

where the dependence on x_S has been omitted for brevity. $\hat{g}_{kj}$ is the unit polarization vector at receiver *j* for ray *k* connecting source and receiver, G_k is the scalar ray propagation term corresponding to the third-order strain Green function, and $E_k = (\hat{p}\hat{g} + \hat{g}\hat{p})/2$ is the second-order ray strain tensor at the

source with $\hat{p}$ the unit phase slowness vector and $\hat{g}$ the unit polarization vector. The symbol : signifies the scalar product or contraction over two indices between tensors. $s(t)$ is the source function, for example a Brune pulse: $s(t) = \omega_c^2 t e^{-\omega_c t}$, $\boldsymbol{M}$ is the second-order moment tensor with six components. Other than the source function, all terms inside the square brackets come from the model and ray tracer. Anisotropy impacts not only the source radiation pattern ($\boldsymbol{E}_k : \boldsymbol{M}$) and receiver polarization vector but also the propagation terms hidden inside G_k – time, spreading and transmission loss, and source and receiver impedance coupling terms. In (1) the sum over rays may include reflections, mode conversions and head waves but presently we consider only direct P, Sh and Sv or "PHV" arrivals. The construction and decomposition of $\boldsymbol{M}$ **is** discussed in a later section.

Inversion

By invoking the isomorphism between second order tensors and vectors, equation (1) can be written in matrix-vector form as $\boldsymbol{d} = \boldsymbol{Gm}$. The inversion of (1) is linear but not necessarily well-posed. For all six elements of $\boldsymbol{M}$ to be resolved a sufficient sampling of the focal sphere (azimuth and take-off angles from the source) is needed (e.g. Eaton, 2010; Vera Rodriguez *et al.*, 2011). This generally requires at least two downhole arrays or an extensive areal distribution of surface and/or shallow grid receivers, or some combination of arrays to provide adequate focal sphere coverage. It is noted that for the case of two vertical downhole arrays as shown later, inversions of events close to the plane defined by the arrays have high uncertainty because the dipole component normal to this plane cannot be resolved. The condition number will be high close to this plane and although condition number is a useful inversion metric, the model covariance matrix is needed to understand parameter resolution.

We solve (1) for the six-vector of moment tensor terms using the generalized inverse, $\boldsymbol{G}^{-g}$, computed using an SVD routine. The previously given form of $s(t)$ is assumed, parameterized by the corner frequency, ω_c. The corner frequency is estimated robustly from the centroid of the particle velocity spectrum of the arrivals, peak displacements are picked and a bandwidth and temporal sampling correction is made that accounts for absorption due to Q. Linear inverse theory (the posterior covariance matrix) provides approximate estimates of uncertainties in the estimated components of $\boldsymbol{M}$, the norm of which serves as a reasonable quality indicator, but the components of $\boldsymbol{M}$ provide little intuition about the nature of the source. To make sense out of $\boldsymbol{M}$ we must decompose it to extract source parameters of interest. The problem of quantifying uncertainties in source parameters will be discussed elsewhere.

Moment tensor decomposition

The impact of anisotropy on event location is well established (e.g. Erwemi *et al.*, 2010), perhaps less well known is that anisotropy local to an event can also distort source attributes of interest (Julian *et al.*, 1998). For example, anisotropy can cause non-double components in the moment tensor, even for a pure slip source, and can rotate TNP axes (the eigenvectors of $\boldsymbol{M}$), altering associated strike, dip and rake angles (Leaney and Chapman, 2010). These distortions can be obviated by decomposing the potency tensor rather than the moment tensor (Chapman and Leaney, 2012). Chapman and Leaney (2012) (eq. 86) write the moment tensor as

$$\boldsymbol{M} = \widetilde{\boldsymbol{M}}_{iso} + \boldsymbol{M}_{DD} = [V]\kappa_{emb}\boldsymbol{I} + \tfrac{1}{2}A[d]\boldsymbol{c} : (\hat{\boldsymbol{d}}\hat{\boldsymbol{n}} + \hat{\boldsymbol{n}}\hat{\boldsymbol{d}}) \qquad (2)$$

where $[V]$ is the volume change due to an isotropic pressure change in a cavity, κ_{emb} is the embedded anisotropic bulk modulus surrounding the cavity, and the second dyadic term describes a moment tensor source due to a displacement discontinuity (DD) across a fracture with unit normal $\hat{\boldsymbol{n}}$. A is the area on the fracture where displacement of total amount (length) equal to $[d]$ has occurred and $\boldsymbol{c}$ is the stiffness tensor at the source. The unit displacement vector $\hat{\boldsymbol{d}}$ need not lie in the plane of the fracture

so that both opening and slip are included in the DD source term. Since opening produces an isotropic moment term, if the source contains opening then the total volume change is split between fracture opening and isotropic pressure change. This is the reason for the $\sim$ over $\boldsymbol{M}_{iso}$ in (2) – it is only part of the total isotropic part of $\boldsymbol{M}$. We note that Vavryčuk (2005) considered focal mechanisms in anisotropic media but considered only the second dyadic DD term in (2).

We seek to recover from $\boldsymbol{M}$ the geometry of the source, free from the distorting effects of anisotropy. In particular, we are interested in recovering $[V]$, $A[d]$, $\hat{\boldsymbol{n}}$ and $\hat{\boldsymbol{d}}$. Chapman and Leaney (2012) describe an algorithm for doing this, the bi-axial potency tensor decomposition. The usual ambiguity remains between fracture normal and displacement vectors, but the angle between them is unique. The opening (or closing) angle comes from $\sin\chi = \hat{\boldsymbol{d}} \cdot \hat{\boldsymbol{n}}$. The volume change or expansion due to an isotropic pressure change $[P]$ in a cavity of volume V is $E = [V] = V[P]/\kappa_{emb} = \widetilde{M}_{iso}/\kappa_{emb}$, determined from the previously estimated $\widetilde{M}_{iso}$. The volume change due to the opening of the fracture is given by $O = 2^{1/2}A[d]\sin\chi$ and the potency or effective volume of the slip term is $S = A[d]\cos\chi$. These comprise a set of "EOS" parameters where the letters stand for $E = Expansion$, $O = Opening$, $S = Slip$. Notice that these all have units of volume or potency, and do not depend on the properties of the medium local to the source as does the moment tensor. In contrast to traditional decompositions (e.g. Hudson *et al.*, 1989) involving a compensated linear vector dipole (CLVD), the elements of EOS are more directly related to the physical modes of deformation expected during hydraulic fracturing.
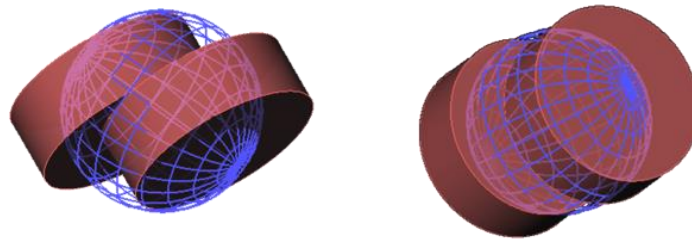

Figure 1. A new 3D graphical representation of a composite source showing oriented EOS effective volumes or potencies. Left: map view, right: side view from south. This synthetic example has significant $-E$=*Expansion* (blue wire frame) and an opening angle of 45° to split $A[d]$ into $+O = Opening$ (thickness of red pucks) and $S = Slip$ (puck displacement). Strike, dip and rake parameters are 60°, 70° and 10°, respectively. Of the two solutions, the one closest to a prior orientation (in this case the true solution) has been chosen for display.

Visualization

Having estimated the moment tensor through an anisotropic inversion and having recovered the source geometry free from anisotropic distortion, we would like to visualize the new EOS source parameters in an intuitive way. Since the EOS parameters are in units of volume we are led to equate them with 3D graphical objects. For example, the volume change due to the isotropic pressure source may be equated with a sphere and the DD part may be equated with a cylinder. Determining a total event volume as a sphere of radius $r_0 = \sqrt[3]{3(|[V]| + A[d])/(4\pi)}$, the radius of the E sphere is defined as $r_E = r_0|[V]|/(|[V]| + A[d])$. The radius of the cylinder is $r_{DD} = r_0 A[d]/(|V| + A[d])$, its height is set to $h = 2r_{DD}|\sin\chi|$ and the cylinder is sliced in half so as to portray slip as the displacement between two "hockey pucks" with slip equal to $s = r_{DD}\cos\chi$. Practically, the limiting case of pure S and no O requires two disks with some minimum thickness so as to be seen from all angles. Colour is used for the sign of E and O, red for expansion and opening, blue for contraction (negative pressure change) and closing. Additionally, the sphere for $[V]$ is drawn with a wire frame with poles along the T axis and the "pucks" are made semi-transparent so the wireframe sphere can be seen inside. Figure 1 shows two

views of the new 3D glyph for a specially chosen source constructed with $-V = A[d]$ and an opening angle $\chi = 45°$ to produce equal parts opening and slip. This is one possible mapping of the new source parameters onto a 3D glyph. Others are possible and have been shown previously, including 3D radiation patterns (Chapman and Leaney, 2012).

Real Data

VTI model calibration. The real data comes from a dual well monitoring job where in each well a 12-level 3C tool was deployed with 100ft receiver spacing. An initial isotropic model was built from sonic and density logs, smoothed and blocked based on a dominant wavelength criterion. Due to a slotted-sleeve completion design perf shots were not available so "ball-drop" or sleeve events were used for calibration (Maxwell *et al.*, 2011). These were distinguished from micro-earthquakes based on observed P polarity as the sleeve events were found to be more directional than a dipole, being well modeled as a horizontal force source pointing towards the heel of the well. A moment tensor inversion was unable to reproduce the observed polarities of sleeve events. Nine such sleeve events were identified with confidence and were used for VTI model calibration. One such event is shown in Figure 2 along with the "VMI" (Velocity Model Inversion) interface. Notice the depth- and hence angle-dependent delay between the Sv arrival (green) and the Sh arrival (red), typical of a VTI medium.
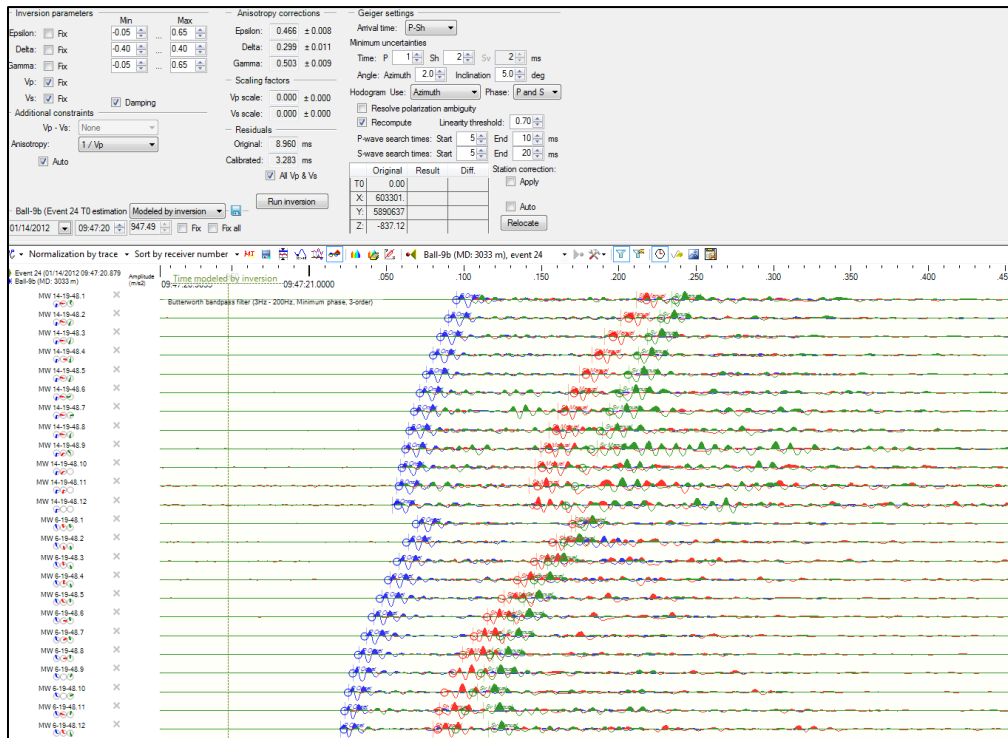

Figure 2. A selected sleeve event about equi-distant to both 12-level monitoring arrays. Waveforms are shown in PHV (qP, Sh, qSv) projection, rotated from the oriented ENU (East,North,Up) frame. PHV=BRG (Blue, Red, Green); the depth- and angle-dependent delay between Sv and Sh is evident. Nine such sleeve events were identified with confidence, arrivals were picked wherever possible and all were used in a linearized inversion for depth-dependent anisotropy parameters. This layered, VTI model reproduces PHV times with an rms residual of 3.3ms, compared to 9ms for the isotropic model.

On each sleeve event P, Sh and Sv ("PHV") arrivals were picked wherever possible, all were then used in a linearized inversion for layered VTI parameters (Mizuno *et al.*, 2010). Since the inversion for VTI parameters in every many layer is impossibly ill-posed, we use a soft, rock-physics constraint wherein the magnitude of anisotropy is driven by an auxiliary log to reduce the parameter space. In sandy-shale / carbonate systems we have found using $1/Vp$ as the auxiliary log practical to drive anisotropy. Using such a constraint keeps the parameter space small and the inverse problem well-posed while yielding physically plausible depth-dependent anisotropy. Figure 3 shows the results of the inversion along with the geometry and rays in 3D for three sleeve event locations. Initial isotropic rms time residuals were 9ms, reduced to 3.3ms after inversion.
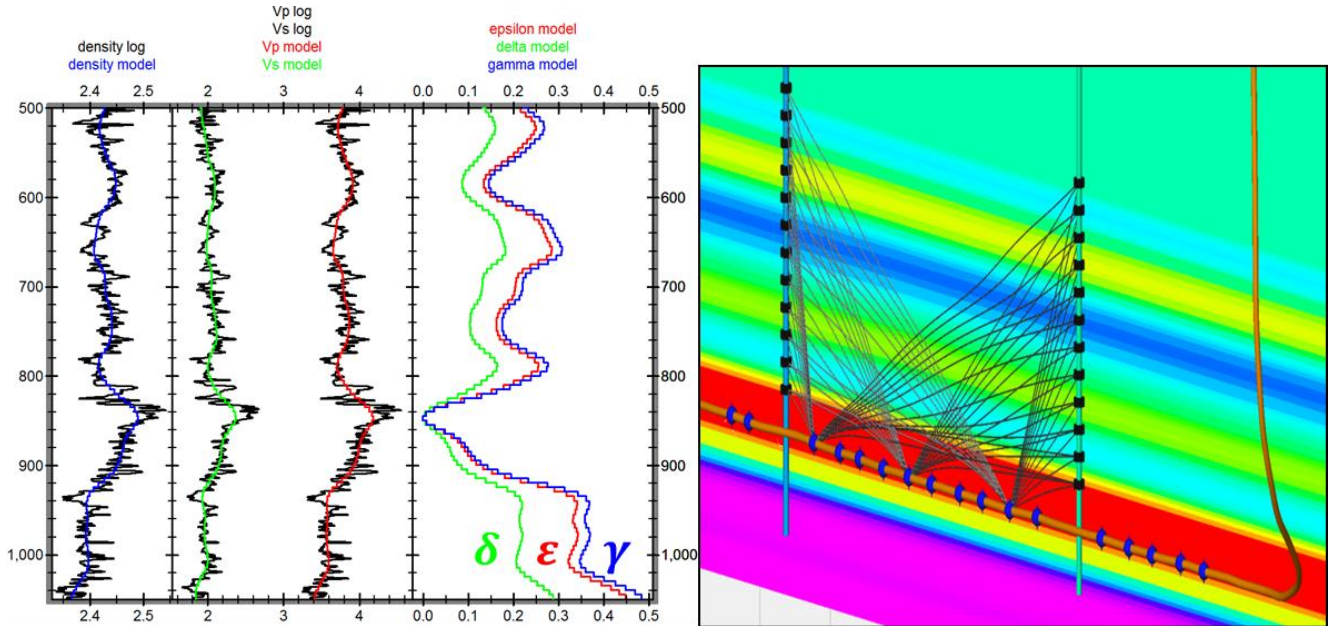

Figure 3. Calibrated VTI model (left) and geometry with P rays from 3 calibration shots (right). Two 12-level arrays were deployed to monitor stimulation from a lateral. Depth-dependent anisotropy follows a soft rock physics constraint. This layered, VTI model reproduces PHV times picked on 9 sleeve "shot" waveforms with an rms residual of 3.3ms.

Moment tensor inversion. Having built and calibrated a layered VTI model (optionally with constant dip), events are detected and located using an algorithm based on a waveform characteristic function (Drew *et al.*, 2005; Michaud and Leaney, 2008). Given location and t_0 an automatic picking algorithm is run on rotated PHV waveforms to extract the peak displacement amplitudes. These may be quality controlled and picks modified or disabled interactively, optionally in a flattened display (Figure 4). Peak amplitude picks are then used with the anisotropic Green functions computed for the event location and equation (1) is inverted for the moment tensor. Figure 5 shows best fit modeled amplitudes with picked amplitudes versus receiver number for an event where the condition number was 8.6 (good). Decompositions are computed and source parameters are shown and PHV radiation patterns are plotted in an equal-area display of the focal sphere along with the sampling provided by the receiver locations. The picked polarity for each phase is colored on each receiver to assess consistency with the inverted radiation pattern. Source parameters can be interactively changed with sliders to examine the impact on radiation pattern. Results are exported to a visualization application. While the process is efficient enough to be run in sequence with event detection and location in real time, the quality depends strongly on the adequacy of the model, signal strength relative to noise, waveform complexity etc. so interactive QC is always recommended.

Multiple event results. Having saved the MTI results they may be visualized in many ways. Standard crossplots are useful but of particular interest is to display results using the new EOS glyph (Figure 1) as a movie so as to appreciate spatio-temporal development. The end of this movie is shown for a central stage with 236 events in Figure 6. Of the two possible orientations the one with fracture plane normal closest to the normal of the events trend (a sub vertical plane striking N45E) has been chosen for display. Mechanisms with a mixture of slip plus opening (red) and closing (blue) components are observed, with a different character (orientation) seen for the events that grew up and out of zone. Interpretation of the results is ongoing.
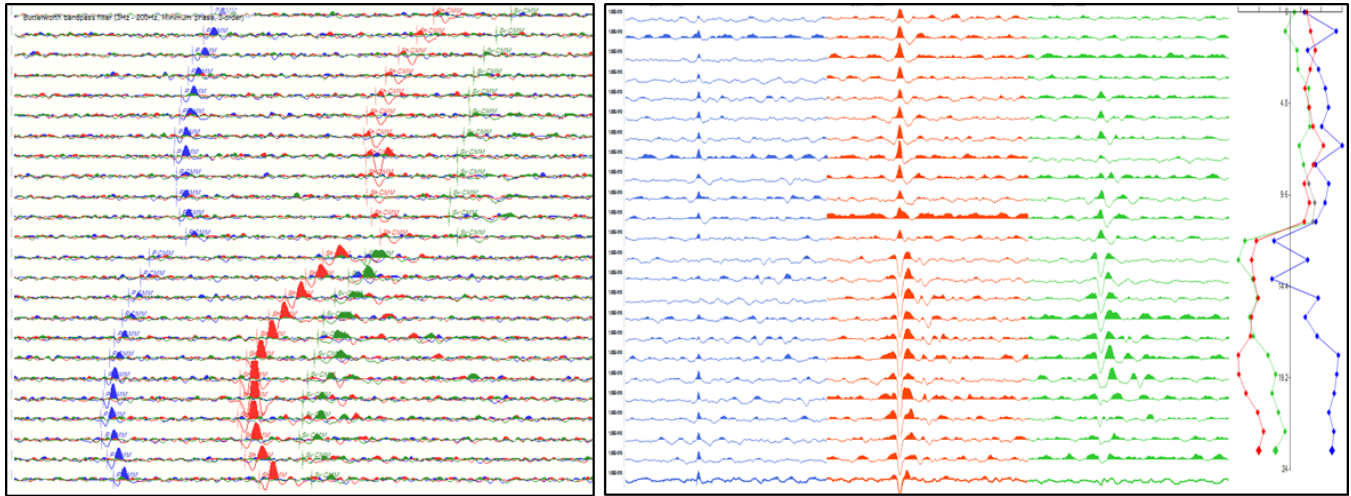

Figure 4. Real event example showing PHV rotated waveforms. Left: in recorded acceleration units with automatic location picks; right: in particle displacement units for the two receiver arrays after flattening on VTI modeled arrival time and manual pick editing. On the far right are shown the peak displacement picks.
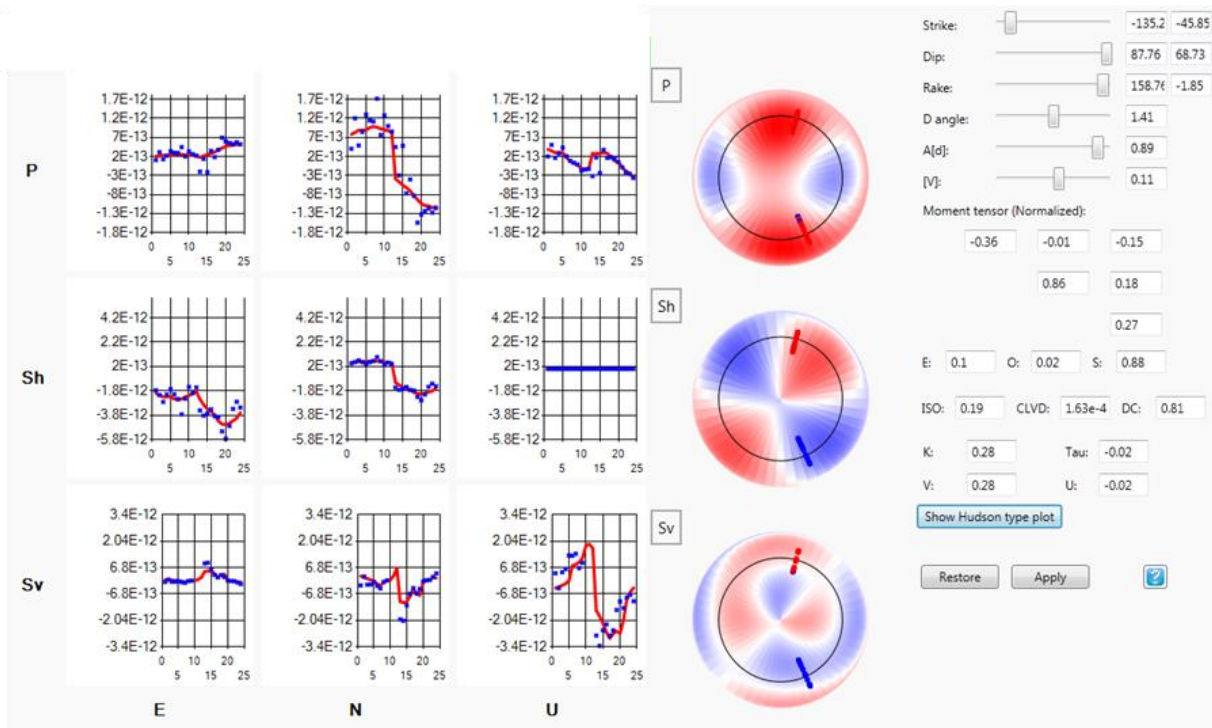
Figure 5. Single event moment tensor inversion results and interactive QC. Left: ENU components of picked PHV amplitudes with best-fit model amplitudes; inverted PHV radiation patterns displayed in an equal area projection with vertical (up) in the center and a ring representing the horizontal plane; right: various normalized decomposition parameters with interactive sliders connected to the modeled amplitude displays on the left.
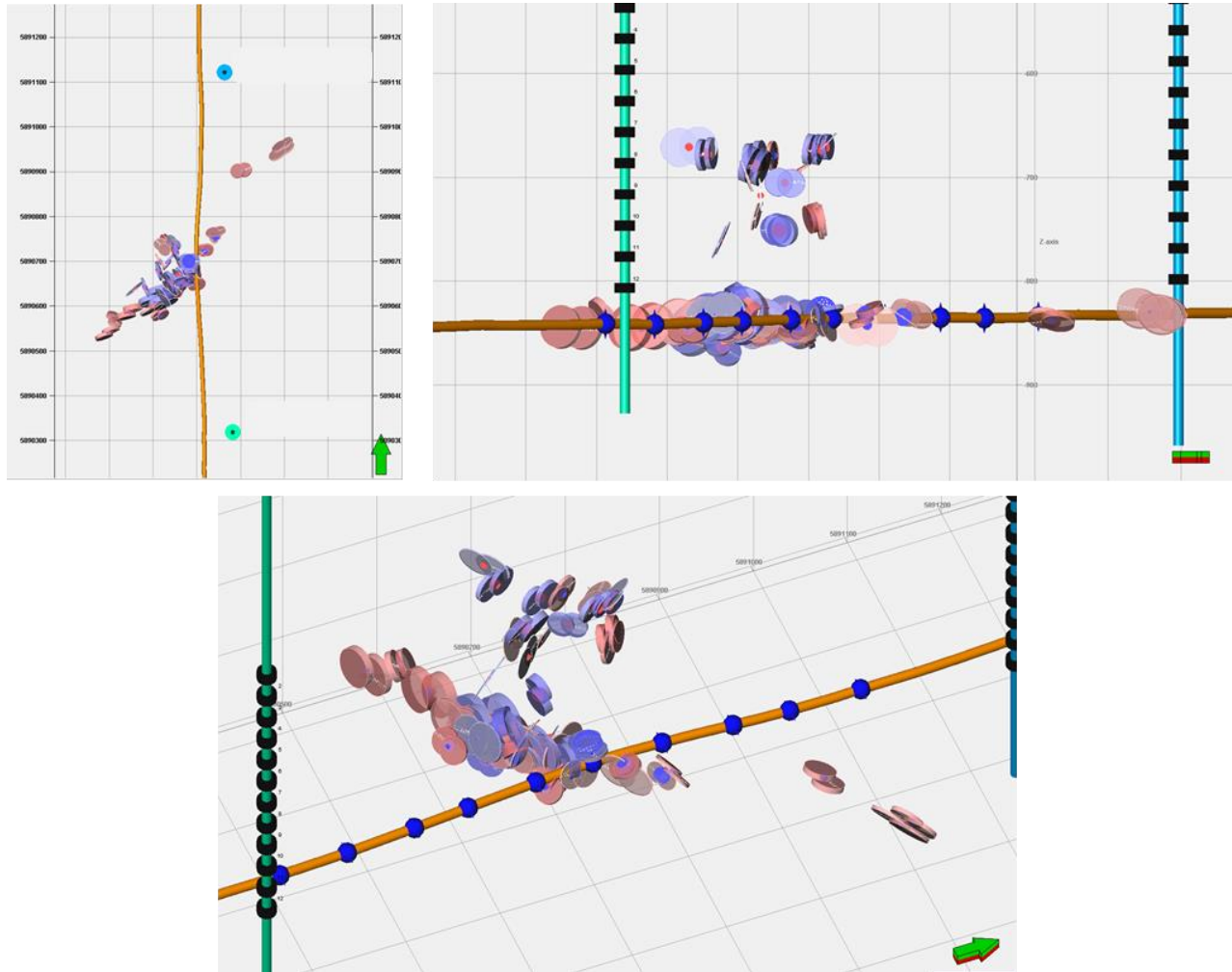

Figure 6. New EOS glyphs for 236 events of a central stage. Left: map view; right: side view from NW, bottom: oblique view from SE. Of the two possible orientations the one with fracture plane normal closest to that of the events trend (a sub vertical plane striking N45E) has been chosen for display.

Conclusions

We have described a time-domain moment tensor inversion method valid for anisotropic media, implemented using a layered VTI ray tracer for Green's function computation. Complementary to the inversion is a new moment tensor decomposition that removes the distorting effect of anisotropy local to the source and a new 3D graphical object to intuitively visualize the results of the decomposition. The new techniques were illustrated on a dual well data set from Alberta where treatments along a lateral were monitored. Critical to the workflow is the calibration of a layered VTI velocity model, and for this a constrained, linearized inversion was run using time picks from nine slotted-sleeve events. Several other stages are available for moment tensor inversion; processing and interpretation is ongoing.

Acknowledgements

References

Chapman, C.H., 2004, *Fundamentals of Seismic Wave Propagation*, Cambridge University Press.

Chapman, C.H. and Leaney, W.S., 2012, A new moment tensor decomposition for seismic events in anisotropic media, *Geophys. J. Int., 188, 343-370.*

Drew, J., Leslie, D., Armstrong, P. and Michaud, G., 2005, Automated microseismic event detection and location by continuous spatial mapping, SPE 95513-PP.

Eaton, D.W., 2010, Resolution of microseismic moment tensors, *SEG Expanded Abstracts*, **28**, 2789-2793.

Erwemi, A, Walsh, J., Bennet, L., Woerpel, C. and Purcell, D., 20120, Anisotropic velocity modeling for microseismic processing: Part 3- borehole sonic calibration case study, SEG Expanded Abstracts, 28, 508-512.

Eisner, L., Williams-Stroud, S., Hill, A., Duncan, P.M. and Thornton, M., 2010, Beyond the dots in the box: Microseismicity-constrained fracture models for reservoir simulation, *The Leading Edge*, **29**, 326–333.

Kim, A., 2011, Uncertainties in full waveform moment tensor inversion due to limited microseismic monitoring array geometry. *SEG Expanded Abstracts*, **29**, 1509-1513.

Julian, B.R., Miller A.D. and Foulger, G.R., 1998, Non-double-couple earthquakes, 1. Theory, *Rev. Geophys.*, **36**, 525-549.

Leaney, W.S. and Chapman, C.H., 2010, Microseismic sources in anisotropic media, 72nd EAGE Extended Abstracts.

Leaney, W.S., Chapman, C.H. and Ulrych, T.J., 2011, Microseismic source inversion in anisotropic media. CSEG Expanded Abstracts.

Leaney, W.S. and Chapman, C.H., 2013, A ray+waveform inversion for the potency tensor. CSEG Expanded Abstracts.

Maxwell, S, Chen, Z., Nizkous, I., Parker, R., Rodionov, Y. and Jones, M., 2011, Microseismic evaluation of stage isolation with a multiple-fracport, openhole completion, CSUG/SPE 149504.

Michaud, G. and Leaney, W.S., 2008, Continuous microseismic mapping for real-time event detection and location, *SEG Expanded Abstracts*, **27**, ?-?.

Mizuno, T., Leaney, S. and Michaud, G., 2010, Anisotropic velocity model inversion for imaging the microseismic cloud, *EAGE Extended Abstracts*.

Nolen-Hoeksema, R.C. and Ruff, L.J., 2001, Moment tensor inversion of microseisms from the B-sand propped hydrofracture, M-site, Colorado, Tectonophysics, 336, 163-181.

Rössler, D., Kruger, F., Psenčik, I. and Rumpker, G., 2007, Retrieval of source parameters of an event of the 2000 West Bohemia earthquake swarm assuming an anisotropic crust, *Stud. Geophys. Geod.*, **51**, 231-254.

Trifu, C-I., Angus, D. and Shumila, V., 2000, A fast evaluation of the seismic moment tensor for induced seismicity, *Bull. Seism. Soc. Am.*, **90**, 1521–1527.

Urbancic, T. I., Trifu, C.-I., Mercer, R.A., Feustel, A.J. and Alexander J.A.G., 1996, Automatic time-domain calculation of source parameters for the analysis of induced seismicity, *Bull. Seism. Soc. Am.* **86,** 1627–1633.

Vavryčuk, V., 2005, Focal mechanisms in anisotropic media, *Geophys. J. Int.*, **161**, 334-346.

Vera Rodriguez I., Gu, Y. and Sacchi, M., 2011, Resolution of seismic-moment tensor inversions from a single receiver array of receivers, *Bull. Seism. Soc. Am.*, **101**, 2634-2642.

Vera Rodriguez, I., Sacchi, M. and Gu, Y.J., 2012, Simultaneous recovery of origin time, hypocenter location and seismic moment tensor using sparse representation theory, *Geophys. J. Int.*, **188**, 1188-1202.